Potential and Pitfalls: On the Use of Transient Absorption Spectroscopy for In-Situ and Operando Studies of Photoelectrodes

Mark Forster,[1] Daniel W.F. Cheung,[1] Adrian M. Gardner,[1] and Alexander J. Cowan[1]*

1. Stephenson Institute for Renewable Energy and the Department of Chemistry, University of Liverpool, Liverpool, L69 7ZD, UK, acowan@liverpool.ac.uk

Key words: Photoelectrode, Photocatalysis, Photoelectrochemistry, Transient Spectroscopy, Operando, In-Situ

Abstract: Here we discuss the application, advantages and potential pitfalls of using transient UV/Vis absorption spectroscopy to study photoelectrodes for water splitting. We revisit one of the most commonly studied water oxidation photoanodes (α-Fe_2O_{3-x}) to provide commentary and guidelines on experiment design and data analysis for TA studies of photoelectrodes within a photoelectrochemical cell. We also assess the applicability of such in-situ TA studies to understand photoelectrodes under operating conditions. A major limitation is that most, if not all, past in-situ TA studies have been carried out using only pulsed light sources to generate carriers, with the electrode held in the dark at other times, which is shown to be a poor model for operating conditions. However, with a simple modification of existing TA experiments a simple operando TA measurement is reported.

I. Introduction:

The use of solar energy to produce storable fuels offers a route to overcoming the intermittency of renewable resources. In particular, light-driven water splitting can be used to generate hydrogen and oxygen, providing a non-fossil-based route to hydrogen. Semiconductor water splitting photoelectrodes have received attention since the initial reports that metal oxides such as TiO_2 are active for this reaction.[1,2] Although significant advances have been made over the last ~50 years the efficiencies of scalable materials for the production of solar hydrogen are still below commonly stated targets.

The basic principles of operation of photoanodes for water oxidation have been reviewed extensively elsewhere and are discussed only briefly here.[3–5] Following photon absorption it is desired that photogenerated electrons are rapidly separated from holes and transported away from the semiconductor-liquid junction (SCLJ) and towards the external circuit, giving rise to current flow. The presence of an electric field (depletion layer) within the semiconductor, close to the SCLJ, also facilitates hole transport to the surface where transfer to the electrolyte i.e. the oxidation of water can occur. However in competition with these two positively contributing pathways exist a range of recombination (loss) pathways both at the semiconductor surface and in the bulk, figure 1b. Whilst the theoretical limit of efficiency of the photoanode (and a photoelectrode in general) may be given by its energetic properties (e.g. positions of the top of the valence band and bottom of the conduction band) the achieved efficiency depends on the balance of rates of the competing contributing and loss pathways.[6,7] The kinetics of these competing processes are dependent on the chemical/physical properties of the electrode, the electric field strength in the electrode (and hence the applied bias) and the photogenerated carrier density (which depends upon the illumination intensity). Therefore, it is important that techniques that can measure the charge carrier dynamics under realistic operating conditions are developed to provide a way to target the development of modified materials with improved solar to fuels efficiencies. Ex-situ studies can provide useful qualitative insights into photoelectrode behaviour and on the role of electrode treatments/modifications. However, they will not provide quantitative data suitable for modelling the electrode under operating conditions. At worst studies carried out under non-operating conditions can even lead to erroneous conclusions being drawn regarding the effect of a particular electrode modification on the underlying mechanism. In this perspective, we critically appraise how transient absorption (TA) spectroscopy has been applied to date to study the kinetics of photoelectrodes, and highlight how few, if any, studies have been reported under true operating conditions.

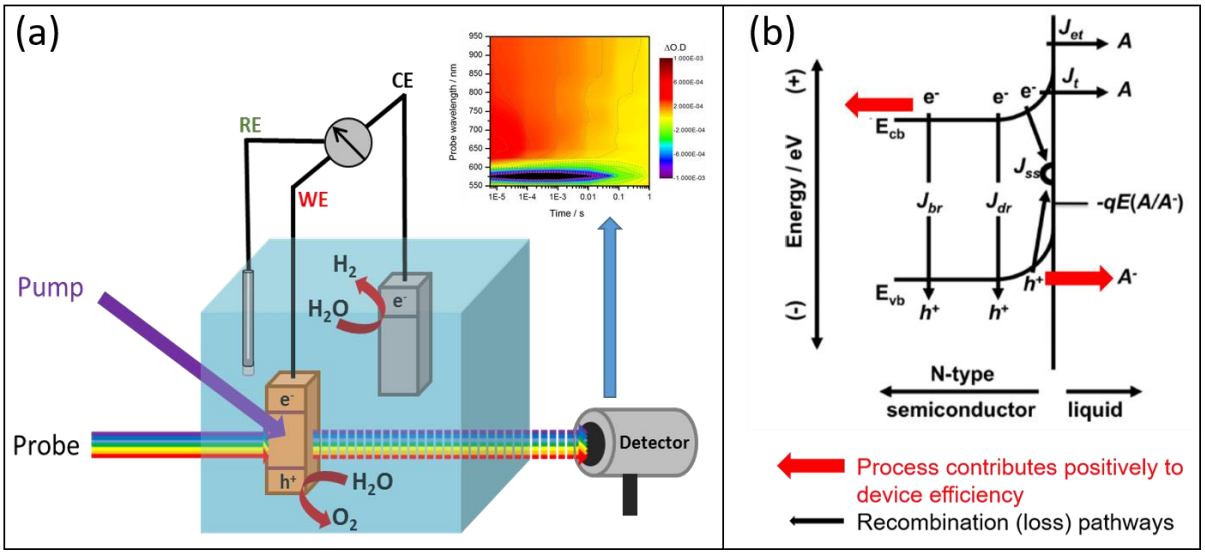

Figure 1. *a) Transient absorption (TA) spectroscopy can be used in-situ to probe charge carriers in photoelectrodes on timescales ranging from femtoseconds to seconds. b) Photoanode internal efficiency is determined by the kinetic competition between positively contributing pathways (red, electron extraction and hole transfer across the SCLJ) and recombination pathways including; bulk recombination giving rise to a current density (J_{br}), recombination in the depletion region (J_{dr}), surface state (trap) mediated recombination (J_{SS}) and electron transfer (J_{et}) and tunnelling (J_t) to intermediates of the water oxidation reaction. Figure 1a adapted from Ref.* [8] *with permission from the Royal Society of Chemistry. Figure 1b adapted with permission from Ref.* [7]*, N. S. Lewis, Inorg. Chem., 2005, 44, 6900–6911. Copyright 2005, American Chemical Society.*

TA spectroscopy is a pump-probe time-resolved technique used to study dynamic processes in materials or chemical compounds. In a TA experiment the change in concentration of species produced following excitation of the sample with a short pulse of light (typically from a laser) is monitored against time, figure 1a. Here we discuss experiments that use UV/Vis absorption spectroscopy as a probe, where the change in optical density (often assumed to be equal to the change in absorbance) or reflectivity, is measured as a function of time. TA spectroscopy using a UV/Vis probe allows for the study of processes with lifetimes as short as femtoseconds (fs), out to seconds, and longer if required. A very recent review provides an overview of the basic principles of TA spectroscopy, alternative probe spectroscopies, and their applications to semiconductor photocatalysts and we do not revisit these points here. Instead, readers interested in the background to pump-probe spectroscopy and its application to photocatalysts are directed there.[9]

TA spectroscopy is being increasingly applied to explore charge carriers within photoelectrodes on both ultrafast (here defined as fs-ns) and slow (μs-s) timescales. The earliest examination of semiconductor materials such as TiO_2,[10,11] WO_3[12] and α-Fe_2O_3[13,14] identified characteristic absorption features which could be assigned to electrons and holes and also gave insights into the nature of processes such as fast

trapping of charges, however, the semiconductors studied were not part of a photoelectrochemical (PEC) cell. To the best of our knowledge the first study of a water splitting photoanode by TA within a PEC cell was carried out on nanocrystalline TiO_2 in 2010 by some of us.[15] In this work it was shown that once a positive bias was applied it was possible to retard electron-hole recombination enough to enable measurement of the kinetics of hole transfer (water oxidation) at the SCLJ. A wide number of photoelectrode materials under an anodic bias within a PEC cell have now been studied using TA spectroscopy[16,17] including; α-Fe_2O_3,[18–20] TiO_2,[15] ZnO,[21] WO_3[22,23]and $BiVO_4$[24–26]. TA spectroscopy has also been used to explore the role of electrode treatments including those designed to passivate/control the distribution of surface states (e.g. thermal annealing steps,[8,22] acid treatments,[27] and overlayers[8,20]), the roles of co-catalysts,[28,29] and heterojunction dynamics.[30–33] In the majority of these studies the kinetics of the charge carriers was found to be strongly dependent upon the applied bias highlighting the benefits of studying photoelectrodes in-situ.

To obtain useful information from such in-situ studies it is important that careful consideration is given to the experiment design and data analysis. Here we re-visit a hematite photoelectrode we have previously studied[8] (α-Fe_2O_{3-x}) in which oxygen deficiencies have been deliberately incorporated into the sample to improve the electronic properties.[34] Our aim is not to re-examine the role of oxygen defects in controlling the structure, but instead to use results from this sample to illustrate practical guidelines to the community for design of in-situ studies. We also aim to demonstrate how with a few simple modifications of widely used TA configurations it is possible to carry out true operando studies of photoelectrodes. To the best of our knowledge, all TA experiments of PEC cells have been carried out using the pulsed laser as the only (or at least dominant) excitation source of the photoelectrode, i.e. the electrode often in the dark except for short (fs-ns) periods of illumination. We define TA studies of photoanodes in a PEC carried out in this way as in-situ. Although the electrode is within the electrolyte and under potentiostatic control it is not under operating conditions due to the lack of CW illumination and at any one time, the photogenerated carrier concentration will not be equivalent to that found during use. In catalysis research operando studies are typically defined as those carried out with simultaneous measurement of catalytic activity (often through detection of products).[35,36] In-line with these criteria here operando TA studies are defined as those only which the photoelectrode is examined whilst operating under both CW illumination and potentiostatic control with a simultaneous measurement the photocurrent. The ability to use the electrical current as a facile measure of catalytic activity represents a significant advantage in the operando study of photoelectrodes. We propose that a move towards operando studies is important if accurate quantitative kinetic modelling of photogenerated charges is to be achieved.

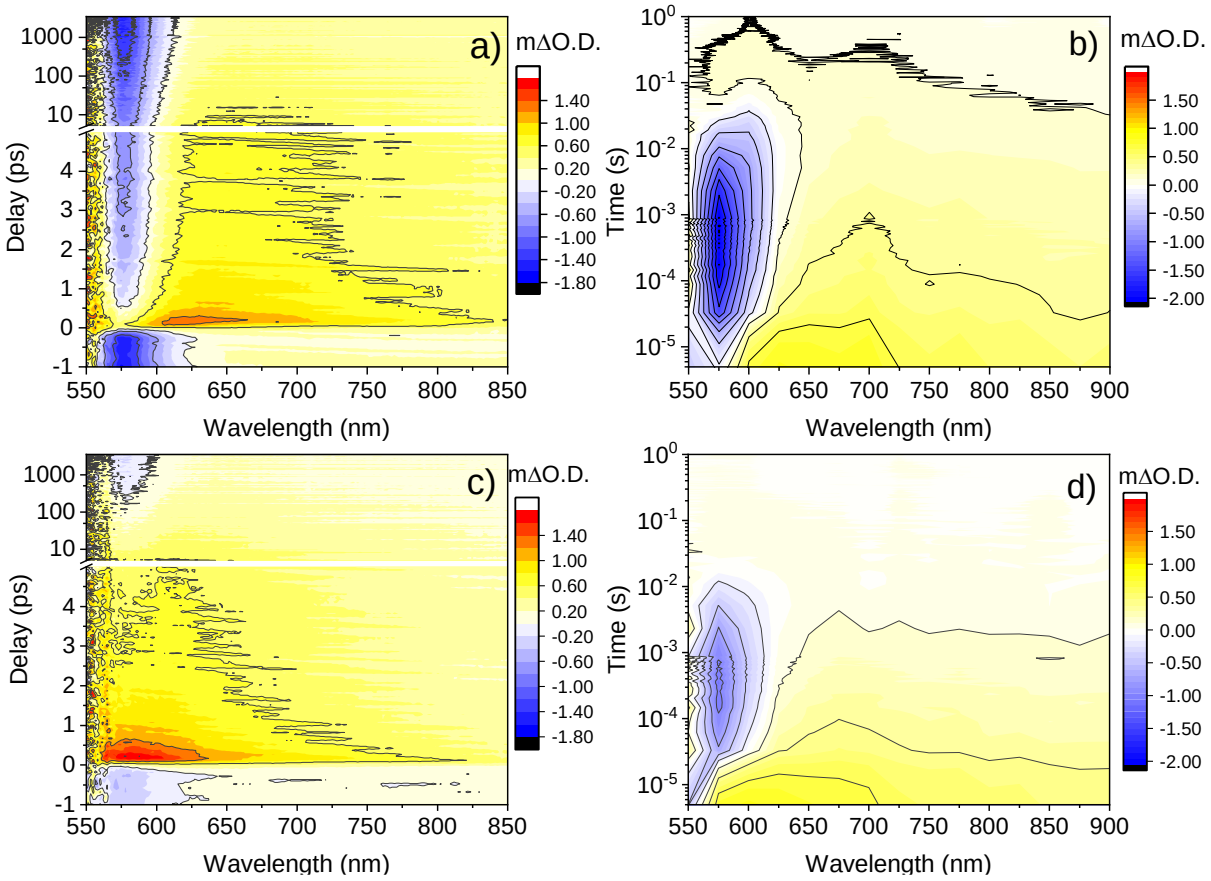

Figure 2. *TA spectra of Fe_2O_{3-x} held at 0.4 $V_{Ag/AgCl}$ in 1 M NaOH electrolyte (a, c) on the ps-ns timescale following 355 nm (21 µJ cm^{-2}, 5 kHz) excitation and (b, d) on the µs-s timescale following 355 nm (200 µJ cm^{-2}, 0.33 Hz) excitation. Experiments (a, b) are recorded in-situ (no CW light source), (c, d) are operando measurements (with an additional CW LED, 365 nm. Data in (a, c) is presented without any correction of negative time delays to show TA signals that are long-enough lived to persist between excitation events.*

II. In-situ TA spectroscopy and assignment of spectral features

TA spectra and selected kinetic traces recorded on both the ps-ns and µs-s timescales of α-Fe_2O_{3-x} collected in transmission mode are shown in figures 2 and 3 and this data will form the centre of the discussion for the remainder of this paper. The experimental apparatus used for the µs-s TA experiments in this study has been described elsewhere,[8] while commercially available apparatus was employed for the ps-ns experiments outlined in ESI. Schematics alongside specific considerations for the instrument design relating to the study of photoelectrodes can be found at figures S1, 2. The transmission UV/Vis spectrum of α-Fe_2O_{3-x} at open circuit is shown in figure 4a. SEM images and the PEC response in 1 M NaOH reported and reproduced here within the supporting information, figures S3,4. A common pump wavelength of 355 nm was chosen for all experiments. Experiments are carried out with front face (α-

Fe_2O_{3-x}, often described as electrolyte/electrode (EE) side) excitation only but we note that an advantage of transmission TA experiments is that comparison of the TA response between EE and SE (substrate/electrolyte) side is possible which can provide insight into the kinetics of charge transport within the electrode and help to discriminate between surface and bulk TA signals in a manner similar to that used previously in transient photovoltage, electrochemical impedance spectroscopy and photocurrent studies.[37,38] Typically for an in-situ TA study, a range of potential steps are recorded, chosen following consultation of the linear sweep voltammogram of the same cell under CW illumination (figure S4) to provide data points both before photocurrent onset and up to the potential where photocurrent plateaus. Here we focus on one particular potential (+0.4 $V_{Ag/AgCl}$) but data recorded at other potentials is shown in figure S5 and we see a strong potential dependence on the kinetics observed.

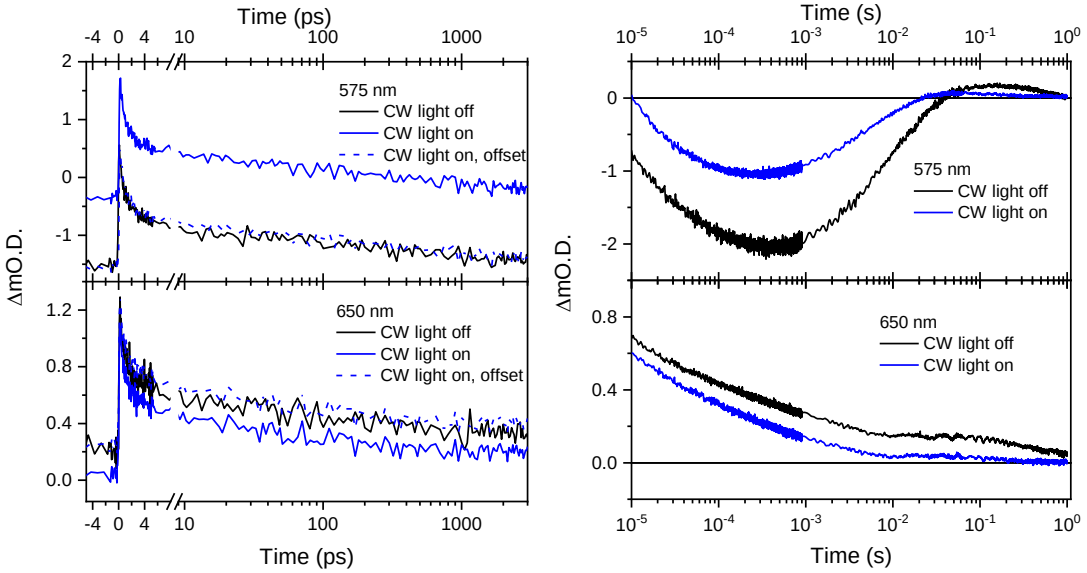

Figure 3. *TA kinetic traces on the ps (left) and μs-s timescale (right) at 575 nm (top) and 650 nm (bottom) following 355 nm excitation of α-Fe_2O_{3-x} held at 0.4 $V_{Ag/AgCl}$ in 1 M NaOH electrolyte. In-situ experiments with no additional CW light are shown in black, operando measurements using a CW LED are in blue. To facilitate comparison between the in situ and operando ps-ns traces, we have applied an offset to the operando traces to align the change in OD at negative times to that of the in situ measurement , denoted "CW light on, offset".*

To assign the observed features in the in-situ spectra to either photogenerated charges, surface intermediates or experimental artefacts (see below) a steady-state spectroelectrochemical study is carried out for the electrode in the same cell using the same potential range studied in the TA experiment, figure 4c. TA experiments provide the user only with a set of difference spectra. Without knowledge of the UV/Vis spectrum of the sample prior to excitation at the applied potential it is not possible to fully understand the difference spectrum. At positive potentials, a strong narrow feature

centred at 575 nm increases in intensity. In a number of past studies, this has been assigned to an electron trap state that lies close (~200 meV) to the conduction band edge which will be partially occupied at open circuit. At positive applied biases these states become oxidised enabling an optical transition to the localised trap states, figure 4c,5b.[8,18,32] A schematic depicting the 575 nm transition can be found in figure S6. A detailed discussion of the transient behaviour of the electron trap state in α-Fe_2O_3 was given by Barroso et al.[18] As at +0.4 $V_{Ag/AgCl}$ the ground state spectroelectrochemistry shows that the electron trap states are partially depopulated, we can make an initial assignment, where the initial small increase in OD at 575 nm (compared to the negative time delays) on the ps timescale is due to fast hole trapping at these trap states in the bulk of the electrode as previously desribed,[18] figure 2a, 3 left. At later times (10-700 μs) the OD at 575 nm then decreases as photoelectrons become trapped in the vacant states within the depletion layer, figure 3 right. Finally, on the ms timescale the trapped electron population decays and the bleach in the TA signal at 575 nm recovers, figure 3 right.

The TA spectra recorded at +0.4 $V_{Ag/AgCl}$, a potential where light-driven water oxidation occurs, also show a broad absorption feature between 550 to 800 nm, that persists for > 0.1 s after excitation, figure 2, 4d. A broad bleach at wavelengths longer than 650 nm can be seen in the ground state (steady state) spectrum at this potential, figure 4c, which could be rationalised by a decrease in free, or only shallow trapped, carriers, but this is contrary to the TA band, figure 4d. In past studies, based on its very long lifetime, combined with the correlation of the amplitude of this signal on the millisecond timescale with the measured photocurrent, the TA response between 600-700 nm has been assigned to be due to photogenerated holes.[39] Here we also make the same assignment.

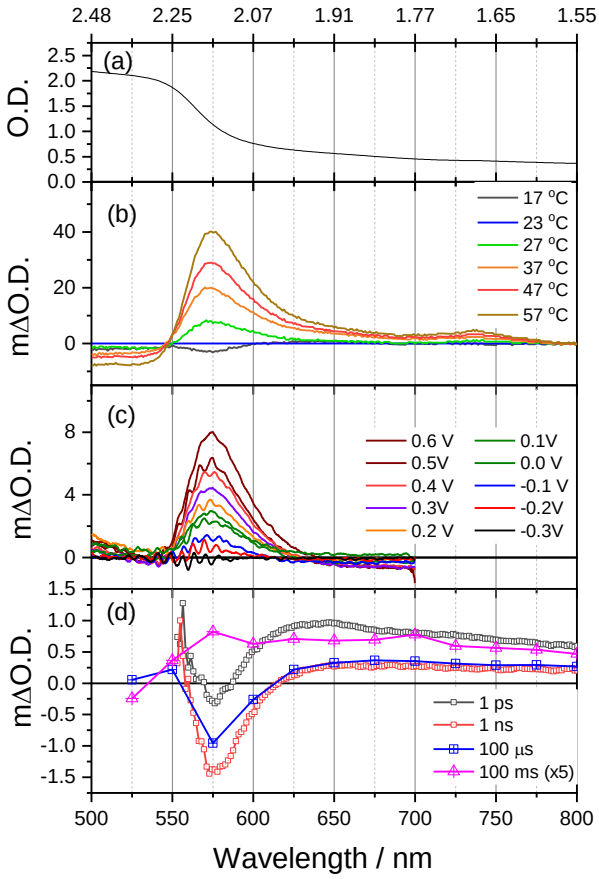

Figure 4. *UV/Vis spectra and difference spectra of α-Fe_2O_{3-x} in 1M NaOH. At open circuit, room temperature (a). Change in optical density of α-Fe_2O_{3-x} held at 0.4 $V_{Ag/AgCl}$ as a function of temperature, data is shown as difference spectra versus 23°C (b). Change in optical density of α-Fe_2O_{3-x} at 23°C as the applied bias is changed with the electrode in the dark versus a potential of -0.3 $V_{Ag/AgCl}$ (c). TA spectra of α-Fe_2O_{3-x} at an applied bias of 0.4 $V_{Ag/AgCl}$ following 355 nm excitation (d). Spectra are at selected timescales and extracted from the data shown in figure 2 in the absence of a CW light source.*

In addition to manual inspection of the TA data and comparison to the spectroelectrochemical response in the dark, global analysis approaches can also be a useful tool to initially identify spectra of individual charge carriers and this is discussed further in section VI. Once initial assignments are proposed, a series of additional experiments can then help to confirm assignments. The use of a hole scavenger, a species that is more readily oxidized than water, such as H_2O_2 can help identify the presence of photogenerated holes and show if they are accessible to the scavenger. For example in-line with other studies here we find that the lifetime of the broad TA feature between 600 and 800 nm is greatly reduced in the presence of H_2O_2 helping confirm its assignment to surface accumulated photogenerate holes, figure S7.[40] Transient photocurrent measurements are also of great benefit and with α-Fe_2O_{3-x} we have previously

shown that the rate of the 575 nm bleach recovery, which we proposed was due to electron detrapping correlated with the rate of charge extraction.[8]

III. Management of thermal contributions

Additional experiments to test the hypothesized assignments to photogenerated species are important as it has been shown that with $BiVO_4$,[41] $LaFeO_3$[42] and α-Fe_2O_3,[43] that thermal effects arising from the laser-induced heating during a TA experiment can give rise to changes in the UV/Vis spectrum which can be difficult to differentiate from excited state absorptions. In one study on α-Fe_2O_3 at open circuit, it was found that the rate of lattice cooling was significantly slower than the rate of electronic relaxation with thermally induced signals dominating on the ns-μs timescales in a TA study.[43] This has led some[17] to raise valid questions about the assignment of spectral features in past TA studies. Therefore we also recommend that the temperature dependence of the UV/Vis spectrum, ideally under applied bias, is reported, something which we are aware of in very few past TA studies.[26] The temperature dependence of the α-Fe_2O_{3-x} photoelectrode at 0.4 $V_{Ag/AgCl}$ in the dark is shown in figure 4b with data presented as a difference spectra versus 23 ^{o}C. The thermal difference spectra observed in figure 4b is consistent with that previously reported by Hayes et al.[43] for an α-Fe_2O_3 film produced from atomic layer deposition. The spectra can be split into 3 sections: features resulting in a reduction in absorption at wavelengths <550 nm, a positive feature centred at 575 nm and a broad positive feature observed at wavelengths >600 nm. The features at wavelengths <550 nm have been assigned to d-d band shifts due to thermally induced structural distortions whilst the thermally induced feature at 575 nm was proposed to originate from both contributions from d-d and the ligand to metal charge transfer (LMCT) transition as a result of DFT calculations.[43] From figure 4 it is clear that the 575 nm band is common in the spectroelectrochemical and thermal study, a conclusion also reached recently elsewhere.[9] It is feasible that the features in the spectra arise from different species, however, given their very similar band shape we believe this to be unlikely, figure S8. Polaron formation, a distortion of the lattice which can occur upon addition (or removal) of excess charge can cause self-trapping, and photoinduced polaron formation is well known to occur with α-Fe_2O_3.[44–46] It has been proposed that the common feature may be a signature of a Fe^{4+} hole polaron.[9] However, experimental evidence against this assignment is that the TA kinetics of the 575 nm band correlates with the rate of electron extraction obtained through simultaneous transient photocurrent measurements, suggesting the state is related to trapped electrons.[8,18] Recent transient extreme ultraviolet[45], transient x-ray[44] and transient visible pump nIR probe[46] measurements have demonstrated the ultrafast (<600 fs) formation of localised electron (Fe^{2+}) polarons, and the lattice distortion following such ultrafast self-trapping may provide a way to reconcile the observed common spectral feature at 575 nm in figure 4. It is apparent that new measurements such

as extreme ultraviolet spectroscopy of photoelectrodes in-situ on a wider-range of timescales (e.g. from fs-ms),will be required to unequivocally settle the debate.

Regardless of the uncertainty arising around the physical nature of the 575 nm trap state, it is clear that it is not possible to disentangle thermal and electronic contributions to the TA response of α-Fe_2O_3 by spectral deconvolution (in the wavelength/O.D domain) alone. Instead, we suggest that the following precautions are taken to enable evaluation of possible thermal relaxation contributions to the TA spectra. Firstly, it is possible to calculate the maximum temperature change following photoexcitation during a TA experiment and use the variable-temperature UV/Vis data to estimate the maximum possible thermal contribution to the TA spectrum. Example calculations are given in the supporting information (figure S9) for the fs and ns laser pulses used here to generate the data in figure 2 and these lead us to conclude that although thermal changes are a likely contributing factor, heating alone following laser excitation is not sufficient to induce the optical changes observed during our TA studies. Secondly the sensitivity of the TA signal to applied bias should also be studied. A straight-forward decrease in ΔOD at 575 nm as the applied potential is made positive would be compatible with decreased radiative recombination at these potentials, in-line with laser-induced heating being the dominant source of the TA response. However here, at potentials where water oxidation occurs the optical density at 575 nm which is increased immediately after excitation, decreases at early times (ps-μs), before increasing (ms) and then decreasing again. In contrast at more negative potentials we see a simple decay in the OD at 575 after excitation. The complex dependence of TA amplitude with time at positive potentials appears incompatible with the signal being solely due to rapid laser-induced heating followed by lattice relaxation. This contrasts the findings of Hayes et al.,[43] where thermal effects swamped the electronic contributions, likely due to the very high laser pulse energies employed (17 mJ cm^{-2} [43] compared to ~31 μJ cm^{-2} employed for the ultrafast experiments reported here). Therefore, we recommend working with the minimum pulse energies possible to minimise heating effects.

As in our example here, where the calculations indicate a contributing factor, decreasing the pump laser energy may in itself be insufficient to remove thermal contributions to the TA spectrum and a balance between the achievable signal to noise and concerns over thermal contributions must be reached. Therefore in addition to checking the sensitivity of the TA signal to the applied bias, the effect of hole/electron scavengers on the TA response, such as that shown in figure S7, S10, should also be studied as the thermal relaxation of the lattice should be insensitive to the presence of small concentrations of chemical scavengers such as H_2O_2 in the electrolyte. Here we find that the TA response at 575 nm on the μs-ms at 0.4 $V_{Ag/AgCl}$ in the presence and absence of H_2O_2 shows differences, again allowing us to be confident that the observed TA signal is dominated by photogenerated charges, figure S10.

IV Validity of in-situ studies to model operational photoelectrodes

Control of the energy of the pump laser is essential, as in addition to causing sample heating it has been shown that the rate of bulk electron-hole recombination is particularly sensitive to pump energy.[47–49] In an attempt to provide kinetic data on photoelectrodes that is relevant to actual operating conditions several studies have stated that laser pulse energies and repetition rates were set so that the photon flux from the pulsed light source is equivalent or less than that experienced under a CW solar simulator at 1 sun.[38,50] Using this approach a correlation between the yield of long-lived electrons and holes measured by TA spectroscopy and the measured photocurrent density under CW illumination has been reported for multiple electrodes.[39,51] In one work using very low pulse energies (35 μJ cm^{-2}, 0.33 Hz) we were even able to quantify charge separation efficiencies within a TiO_2 electrode using TA spectroscopy with results that matched those achieved through more conventional CW incident photon to current efficiency measurements.[38] However, whilst it is clear that such in-situ TA experiments can provide insights into the mechanisms of operational PEC cells it must be recognised that the very high peak laser powers achieved using short fs-ns pulses make a pulsed laser a poor model for solar illumination. Typically, for slow TA experiments (ns-s)[18] a weak CW probe light is present, but this is usually monochromatic light of photon energy below the band gap. In ultrafast (fs-ns) measurements a white light probe is generated but this too is pulsed. Therefore, the dominant (or in many cases sole) excitation source is the pulsed laser. Excessive geminaterecombination may be controlled through decreasing the pulse energy, but the use of a very short pulsed light-source alone is still likely to lead to kinetics being measured which are not representative of the electrode under operating conditions. CW illumination generates non-equilibrium charge carrier concentrations with the magnitude of quasi-electron and hole Fermi level splitting being dependent on the CW light intensity. Therefore recombination dynamics, distribution of surface intermediates, surface state occupancies and double-layer structures are expected to be dependent on steady-state illumination intensity.

Insight into the importance of carrying out experiments under operating conditions comes from photoinduced absorption (PIA) spectroscopic studies of photoelectrodes, particularly from the Durrant group. [52–55] In a PIA measurement the UV/Vis absorption spectrum of the photogenerated holes is measured to derive the surface hole concentration (h_s^+) and simultaneously the photocurrent density (J^{ph}) is recorded allowing for the derivation of the rate law for water oxidation, using equation 1 where α is the order of the water oxidation reaction with respect to surface hole density and k_{wo} the water oxidation rate constant.

$$J^{ph} = k_{wo} \cdot (h_s^+)^{\alpha} \qquad \text{Equation 1.}$$

Consistently in these studies Durrant *et al.*, have observed that the rate of hole transfer into the electrolyte (the rate of water oxidation) is dependent upon surface hole density and that two distinct mechanisms can occur, again dependent upon the surface density of holes.[53] For α-Fe_2O_3 a transition

from first-order ($\alpha = 1$) to third-order kinetics with respect to surface hole concentration occurs. In the third-order mechanism, two nearest neighbours are triply oxidised prior to O-O bond formation. This is important as the need to accumulate three holes at the reaction site means that, although this mechanism dominates under typical operating conditions (1 sun CW), during TA experiments only a first-order mechanism that proceeds *via* a series of one-hole oxidation steps without the need to accumulate oxidised intermediates occurs.[51] Therefore TA spectroscopy has been previously blind to the presence of the 2nd mechanism and the lifetime of holes during water oxidation measured by past in-situ TA studies are significantly longer (typically 0.3 to 3 s for α-Fe_2O_3)[11,12,18,24,51] than those under 1 sun and therefore should be treated with caution.

PIA is a powerful tool to measure water oxidation kinetics, but it provides limited information on the faster processes that may be occurring within the electrode (e.g. charge trapping, bulk-recombination) therefore to demonstrate the effect of CW illumination more widely on electron-hole kinetics we have repeated the TA experiments of α-Fe_2O_{3-x} under CW illumination, figure 2,3. All experiments are reported at 0.4 $V_{Ag/AgCl}$ as at this potential a significant (*ca.* 0.35 mA cm^{-2}, figure S4, 11, 12) steady state photocurrent is measured. Figure 3 shows that the ultrafast TA kinetics (ps-ns) in the presence of the CW light source. The change in OD at negative time delays in the ps-ns TA data are due to processes that occur on timescales slower than the laser repetition rate (10 kHz probe) being sensitive to the CW light which become evident from inspection of the μs-s TA spectrum. In some studies ultrafast TA data is shown normalised with the change in OD being set to zero at negative time delays and we highlight the need to avoid this. A limitation of many ultrafast TA measurements of photoelectrodes that use high repetition rate laser systems is that equilibrium is not reached between each laser shot. Observation of a non-zero change in optical density at negative time delays is an important indicator of the presence of long-lived species and as is shown here the negative time data can provide useful insights into the slow processes. On the ultrafast timescale the kinetic traces recorded at 650 nm, and 575 are near indistinguishable, showing the same initial decay rates. Several potential conclusions can be drawn here. Firstly it is possible that laser-induced heating is dominating the TA spectrum on the ultrafast timescale and that the addition of a CW light source does not change the rate of thermal relaxation, however, as calculated above the magnitude of the observed TA response is greater than that achievable through heating alone. Alternatively, it can be concluded that the TA signals on these timescales are dominated by charge carriers in the bulk and that as the electrode is under potentiostatic control the bulk electronic properties are not significantly changed by the CW light. It is also possible that the high peak laser powers of the fs-ns pulses used lead to carrier injection levels so large that the CW light has a negligible effect on the excess carrier population at a given time and this represents a common shortcoming of many fs experiments.

In contrast to the ultrafast study, we find that the lifetime of the TA signal at all wavelengths is significantly reduced under CW illumination in the slow (μs-s) operando TA experiment, figure 2, 3. Fitting of this data to obtain kinetic parameters for individual processes is discussed in the following section. However, even without fitting, a simple comparison of the magnitude of the TA signals with and without CW illumination we find that there is an ca. 85% reduction in hole signal at 650 nm at very long times (0.1 s after excitation), in line with the findings from the past PIA experiments described above, figure 3. The electron trap signal at 575 nm is also found to be sensitive to the CW light source on the μs-ms timescale with accelerated trapping and de-trapping from the surface trap states occurring under LED illumination, figure 3.[8] The large changes in the kinetics of the charges on the slow timescales highlights the importance of carrying out operando studies. Perhaps unsurprisingly this study indicates that the photoelectrode surface is markedly different under pulsed and CW illumination.

V. Fitting of photoelectrode charge carrier kinetics

Analysis of the kinetic data provides a way to extract kinetic parameters to construct models of the charge carrier kinetics and, in some cases generate the spectra of transient species associated with a decay process. The simplest way to analyse the TA data is to fit kinetic data recorded at selected wavelengths independently. For example, here it might be considered appropriate to only fit the kinetics of the photogenerate hole (650 nm) and electron trap state (575 nm). In this case, each trace is fitted, to a pre-determined combination of functions (e.g. combinations of exponential and power-law functions). A review that describes the fitting of photoelectrode TA data in this way has been recently published.[9] While such an approach is straightforward to implement and has been most widely used for photoelectrode studies,[29,51,56,57] we advise against considering the kinetics of only one or two wavelengths in isolation. Reducing the entire TA data set to one or two kinetic traces runs the inevitable risk of arriving at an over simplified kinetic model for the photoelectrode. Furthermore, the number and type of fitting functions is determined by the user, often by the assumption of a particular kinetic model occurring. Whilst a thorough study should assess the quality of fit for multiple kinetic models, few works on photoelectrodes have presented this data and we need to recognise the potential danger of confirmation bias leading an investigator to seek a fit to their preferred model.

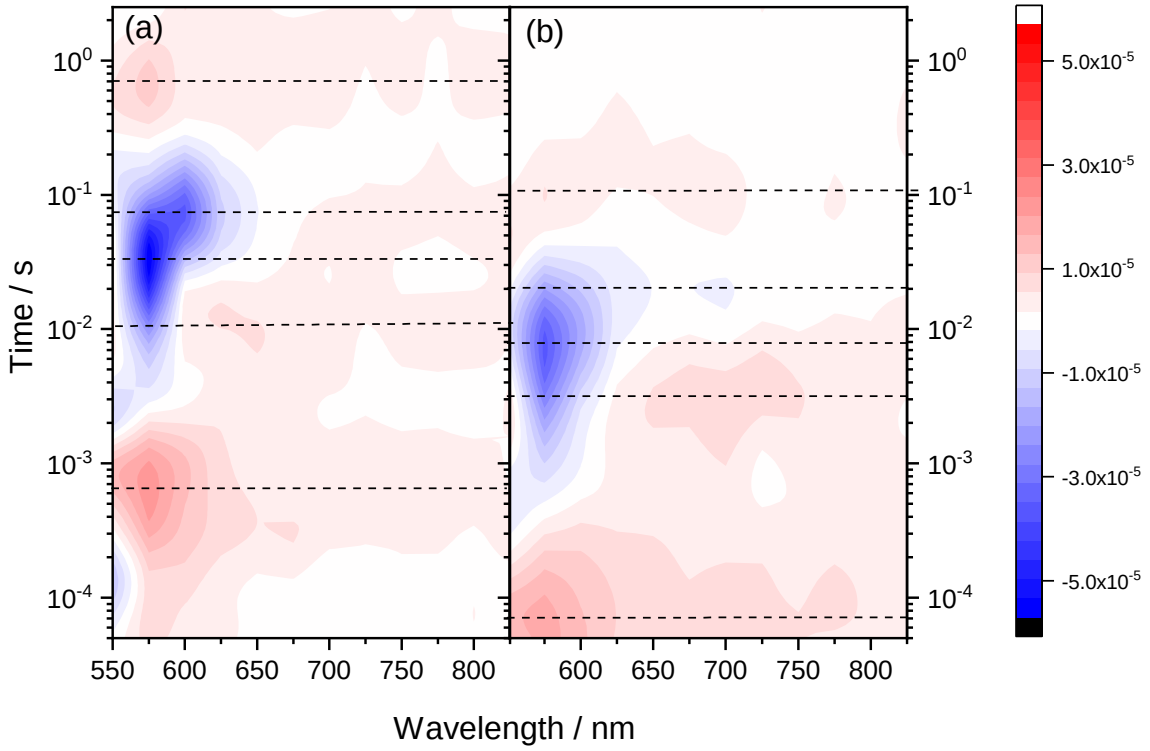

Figure 5. *LDM generated from the TA data shown in figure 2b,d of α-Fe_2O_{3-x} held at 0.4 V following 355 nm excitation in the dark (in-situ study, a) and under CW illumination (operando study, b). The dotted lines indicate the 5 lifetime distributions identified for each study.*

Alternatively, global fitting procedures such as global lifetime analysis (GLA) offers a way to assess all wavelengths simultaneously.[58] In GLA all kinetic traces are simultaneously fitted to a discreet, often small (2-5), number of exponential functions, with the pre-exponential factors allowed to vary across the wavelengths. Such an approach allows for the construction of decay associated spectra (DAS) for each lifetime component which are a plot of the pre-exponential factors versus wavelength, providing a composite of the spectra of the species contributing to that particular kinetic process. A number of examples[59,60] of the application of GLA exist being applied to photoelectrodes including a TA study of $BiVO_4$ on the kinetics of charge trapping on the ultrafast timescale.[25] In a similar approach to GLA it is also possible to carry out a global analysis by spectral fitting where TA data is fitted to a discreet number of component spectra with the amplitude allowed to vary for each across the time slices. This approach has been used in a study on oxygen deficient WO_3 photoanodes where singular value decomposition was used initially to extract spectral components prior to amplitude weighted fitting.[23] Global fitting methods such as GLA can be used without a priori knowledge of the number of experimental decays or spectral components and when combined with target modelling can be used to test specific kinetic

models.[58] However, photoelectrodes present a challenge for GLA due to their complex kinetics and the often time-dependent spectra of semiconductor excited states which continue to evolve over prolonged periods. The presence of multiple species (free carriers, trapped carriers, surface intermediates) which react via a range of different pathways are not easily captured using only a small discreet number of exponential functions and solutions obtained can appear similar. A further complication is that common nanostructured photoelectrode materials contain high levels of defects and a wide distribution of trap and reaction sites. Therefore, single exponential functions are often a poor fit to the kinetics of a single pathway. In photoelectrode TA studies where the kinetics at single wavelengths have been fitted the heterogeneity of sites has been partially accounted for through the use of stretched exponential functions with the stretching parameter providing useful insights into the photoelectrode.[1,15] We are not aware of the implementation of stretched exponential functions within the GLA procedure, however this would represent an interesting route to aid the analysis of photoelectrode TA data.

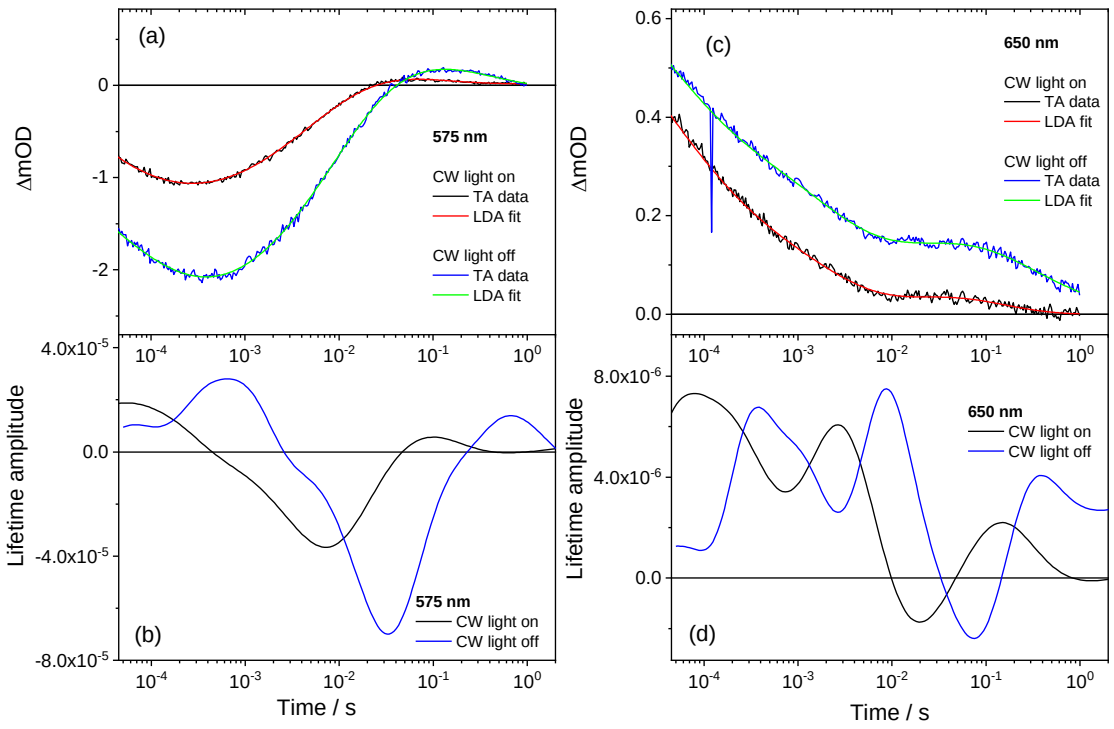

Figure 6. *LDA fits (red, green lines) to the experimental TA data (blue, black) at 575 nm (a) and 650 nm (c) for a α-Fe_2O_{3-x} photoelectrode held at 0.4 V in 1 M NaOH following 355 nm excitation. The lifetime distribution at these specific wavelengths is shown in (b,d). It is noticeable that a similar pattern in lifetime distributions exist but that under CW illumination (black lines) the lifetimes are significantly decreased.*

Instead here we demonstrate the use of lifetime density analysis (LDA) to study photoelectrode kinetics. LDA is a powerful technique for analysing complex kinetic data and it has been applied to a number of fields including TA studies on light-harvesting photosynthesis,[61] photo-switches[62] and photoconductive hydrogels.[63] Despite its potential advantages, we do not believe it has been applied to photoelectrodes previously. LDA is based on the principle that TA spectroscopic data (ΔA, which here we approximate to ΔOD) can be represented by the integral of a continuous distribution of single exponential functions, Eq 2.

$$\Delta A\ (t,\lambda) = \int_0^\infty \Phi(t,\lambda) e^{-t/\tau}.\delta t \qquad \text{Equation 2}$$

To make equation 2 readily addressable LDA approximates the integral to a semi continuous sum of a large number (typically $n > 100$, here we use n = 200) of exponential functions which are evenly distributed across the timescale. Typically experimental detail will also be convoluted (⊗) by an instrument response function (IRF(t,λ)), leading to equation 3.

$$\Delta A\ (t,\lambda) = \sum_{j=1}^{n} x_j(\tau_j,\lambda)\, e^{-t/\tau_j} \otimes IRF(t,\lambda) \qquad \text{Equation 3}$$

Equation 3 indicates that LDA and GLA are similar, different only in the value of n (LDA >100, GLA typically ~2-5). However, a significant advantage of LDA is that it is effectively a model independent fitting process with no user input into the expected number of pathways. As a model free fitting process it is important to note that the equation 3 is not based on the underlying kinetic equations governing the photoelectrode, but it is instead designed to provide an initial visualisation of common lifetime components without assumption as step towards construction of a kinetic model. Furthermore, the very large number of functions available makes it particularly amenable to complex and dispersive kinetics. LDA results are usually shown as lifetime density maps (LDM) where the amplitude (x_j) for each lifetime is plotted on the z-axis of a x-y surface of wavelength versus lifetime (τ_j), figure 5. A LDM provides a simple visualisation of the number of kinetic processes occurring, indicated by peaks in the LDM with positive and negative values indicating a lifetime component that is leading to a decrease or increase in ΔA respectively. The distribution of lifetimes associated with each peak can give important information, for example, it may potentially inform on the distribution of a particular trap-state within a material or provide insights into carrier transport mechanisms. However before drawing conclusions relating to lifetime distributions it is advisable to consider the limitations and assumptions of the regularization procedure used within the LDA analysis and a summary of these is reported elsewhere[64,65]. Regularization is required as the large number of parameters makes over fitting a concern. Fitting of un-regularized spectra leads to fitting to the noise, therefore procedures to penalise the use of large coefficients of fitting are required, effectively smoothing the data. Here we present an LDA of the TA spectra of α-Fe_2O_{3-x} recorded on the μs-s timescale both in the presence (operando) and absence (in-situ) of the CW light source, figure 5. Freely available software packages for LDA are now

available[64,66] and here we used OPTIMUS which employs a Tikhonov regularization and the appropriate regularization parameter (α) was chosen from the point of maximum curvature of the L-curve, available as figure S13, 15. Full details of the fitting parameters, fits to all wavelengths and reconstruction of the TA contour maps are available in the supporting information figures S13-16.

Figure 5 shows at least 5 lifetime distributions, indicated by the dashed lines, within the TA data on the μs-s timescale demonstrating the complexity of the charge carrier dynamics on this timescale. It is also worth noting that a limitation of the Tikhonov regularization is that it can lead to broadening of kinetic distributions making it hard to identify close lying distributions of lifetimes so it is feasible more lifetime distributions are present than the 5 identified.

The aim of this perspective is to provide guidelines and to critically appraise current experiment and data analyses methodologies used in the TA spectroscopy of photoelectrodes. A future study will focus on the assignment of each lifetime distribution and the development of a complete kinetic model. Here we only briefly outline a few features to demonstrate the potential of LDA for operando studies of photoelectrodes. Firstly, the LDM maps also allow for the identification of new spectral features and kinetic pathways not previously included in past kinetic models. In the absence of CW illumination the lifetime distribution centred around 640 μs, which has a strong contribution to the TA data between 550 and 625 nm, can be assigned to surface trapping of electrons, figure 5a, 7a, b. The recovery of the bleach signal across this region (indicated by the negative amplitude lifetime clusters between 1-100 ms), is markedly different at 575 nm and 600 nm which we propose is due to the presence of a 2nd trap state with a TA spectrum with a maxima around 600 nm, figure 5. Further experiments are required to confirm the nature of this TA band but its identification through the use of LDA highlights the benefits of the application of this procedure to TA studies of photoelectrodes. The LDA analysis also allows us to test the validity of our claim to be carrying out a true operando study through comparison of the measured lifetime of the surface hole in the TA studies to the rate of hole transfer measured by PIA. The lifetime of holes taking part in water oxidation can be assumed to be the longest-lived feature around 650 nm in the LDM. In the absence of a CW light the LDM shows a distribution centred at 0.40 s, with a significant tail of lifetimes to beyond 2 s in-line with previous TA studies,[39,51] figure 6. The peak at 0.4 s indicates that initially the third-order water oxidation may occur, however as the electrode is in the dark after the laser excitation the surface hole density rapidly decreases and a switch to the slower first-order mechanism occurs, giving rise to the very long lifetimes (>1 s), figure 5a, 7c,d.[53] In contrast under CW illumination the hole lifetime is significantly decreased and a single distribution centred at 0.14 s (7.1 s^{-1}) is present, indicating that under CW illumination only the third-order mechanism is occurring. The measured rate of hole transfer in our operando TA study is in excellent agreement to the PIA measured hole turnover frequency for α-Fe_2O_3 at approximately 1 sun condition (*ca.* 4 s^{-1})[53] confirming the validity of our claim to be carrying out operando TA spectroscopy.

VI. Concluding remarks and guidelines

Table I. *Guidelines for TA studies of photoelectrodes*

Recommendation	**Details**
Adoption of a standard terminology to explain the experimental conditions	In-situ: electrode at an applied potential within a PEC cell Operando: At an applied potential within a PEC cell and under CW light with simultaneous measure of photocurrent or chemical products
Reporting of steady-state spectroelectrochemical response of electrodes as standard	Essential for both in-situ and operando studies to enable analysis of TA spectra. It is proposed that reviewers should question the absence of this data
Assessment of thermal contributions to the TA spectra	Variable temperature steady state UV/Vis allows for calculation of the maximum contribution to the TA spectra - Where thermal contributions are shown to be a potentially significant contributor analysis of the dependence of the TA spectra on applied potential, CW light and chemical scavengers can provide evidence for the presence of photogenerated species
Operation at lowest practical laser pulse energies	Helps minimise heating and provide a closer model to solar illumination, minimising excess bulk electron-hole recombination
Use global analysis procedures, ideally model independent, to analyse/fit kinetic data	LDA is found to be particularly suitable for photoelectrodes due to its ability to handle complex dispersive kinetics

The development of new more efficient photoelectrodes for water splitting is a pressing goal that requires input from a broad range of expertise. In presenting a revised study of α-Fe_2O_{3-x} we have re-examined many standard practices used during TA studies of photoelectrodes. This has led to the generation of a series of best practice recommendations designed to ensure that results generated are of greatest benefit to the wider solar fuels community and these are summarised in table 1. Of these, we highlight the need to clearly indicate to the community the conditions, and hence the limitations, of a particular study and definitions are proposed based on common terminology used within the catalysis community. TA studies of photoelectrodes in the dark (in-situ) have great value, providing relevant data on bulk carrier kinetics and charge separation yields. However, recent PIA experiments and the work presented here shows that experiments carried out in the dark with only short-pulsed excitation lead to unrealistic surface and double-layer conditions. Therefore, we look forward to more future studies being carried out under true operando conditions which when coupled with appropriate data analysis protocols will enable the accurate, quantitative kinetic modelling of photoelectrodes.

Acknowledgements: Professor Yat Li (UCSC) is thanked for the α-Fe_2O_{3-x} sample. The Imaging Centre at Liverpool (ICaL) is thanked for access to STEM. Financial support for this works is from the INTERREG Atlantic Area programme (Grant reference EAPA_190_2016) and the EPSRC (EP/P034497/1). The EPSRC is also acknowledged for equipment funding (EP/S017623/1).

Data availability statement: The data that support the findings of this study are available from the corresponding author upon reasonable request.

Supplementary material: See the supplementary material for a description of the experimental methods and apparatus, electrode characterisation data, calculations of the thermal contributions to the TA spectra and supporting figures for LDA.

VII. References

1 P. J. Boddy, *J. Electrochem. Soc.*, 1968, **115**, 199–203.

2 A. Fujishima and K. Honda, *Nature*, 1972, **238**, 37–38.

3 M. G. Walter, E. L. Warren, J. R. McKone, S. W. Boettcher, Q. Mi, E. A. Santori and N. S. Lewis, *Chem. Rev.*, 2010, **110**, 6446–6473.

4 Y. He, T. Hamann and D. Wang, *Chem. Soc. Rev.*, 2019, **48**, 2182–2215.

5 C. Ros, T. Andreu and J. R. Morante, *J. Mater. Chem. A*, 2020, **8**, 10625–10669.

6 H. Gerischer, *J. Electroanal. Chem.*, 1983, **150**, 553–569.

7 N. S. Lewis, *Inorg. Chem.*, 2005, **44**, 6900–6911.

8 M. Forster, R. J. Potter, Y. Ling, Y. Yang, D. R. Klug, Y. Li and A. J. Cowan, *Chem. Sci.*, 2015, **6**, 4009–4016.

9 T. J. Miao and J. Tang, *J. Chem. Phys.*, 2020, **152**, 194201.

10 D. Bahnemann, A. Henglein, J. Lilie and L. Spanhel, *J. Phys. Chem.*, 1984, **88**, 709–711.

11 J. W. Tang, J. R. Durrant and D. R. Klug, *J. Am. Chem. Soc.*, 2008, **130**, 13885–13891.

12 F. M. Pesci, A. J. Cowan, B. D. Alexander, J. R. Durrant and D. R. Klug, *J. Phys. Chem. Lett.*, 2011, **2**, 1900–1903.

13 A. G. Joly, J. R. Williams, S. A. Chambers, G. Xiong, W. P. Hess and D. M. Laman, *J. Appl. Phys.*, 2006, **99**, 053521.

14 G. Xiong, A. G. Joly, G. P. Holtom, C. Wang, D. E. McCready, K. M. Beck and W. P. Hess, *J. Phys. Chem. B*, 2006, **110**, 16937–40.

15 A. J. Cowan, J. W. Tang, W. H. Leng, J. R. Durrant and D. R. Klug, *J. Phys. Chem. C*, 2010, **114**, 4208–4214.

16 D. V. Esposito, J. B. Baxter, J. John, N. S. Lewis, T. P. Moffat, T. Ogitsu, G. D. O'Neil, T. A. Pham, A. A. Talin, J. M. Velazquez and B. C. Wood, *Energy Environ. Sci.*, 2015, **8**, 2863–2885.

17 K. E. Knowles, M. D. Koch and J. L. Shelton, *J. Mater. Chem. C*, 2018, **6**, 11853–11867.

18 M. Barroso, S. R. Pendlebury, A. J. Cowan and J. R. Durrant, *Chem. Sci.*, 2013, **4**, 2724–2734.

19 Z. Huang, Y. Lin, X. Xiang, W. Rodríguez-Córdoba, K. J. McDonald, K. S. Hagen, K.-S. Choi, B. S. Brunschwig, D. G. Musaev, C. L. Hill, D. Wang and T. Lian, *Energy Environ. Sci.*, 2012, **5**, 8923.

20 T.-P. Ruoko, A. Hiltunen, T. Iivonen, R. Ulkuniemi, K. Lahtonen, H. Ali-Löytty, K. Mizohata, M. Valden, M. Leskelä and N. V. Tkachenko, *J. Mater. Chem. A*, 2019, **7**, 3206–3215.

21 R. L. Willis, C. Olson, B. O'Regan, T. Lutz, J. Nelson and J. R. Durrant, *J. Phys. Chem. B*, 2002, **106**, 7605–7613.

22 S. Corby, L. Francàs, A. Kafizas and J. R. Durrant, *Chem. Sci.*, 2020, **11**, 2907–2914.

23 S. Corby, E. Pastor, Y. Dong, X. Zheng, L. Francàs, M. Sachs, S. Selim, A. Kafizas, A. A. Bakulin and J. R. Durrant, *J. Phys. Chem. Lett.*, 2019, **10**, 5395–5401.

24 Y. Ma, S. R. Pendlebury, A. Reynal, F. Le Formal and J. R. Durrant, *Chem. Sci.*, 2014, **5**, 2964.

25 J. Ravensbergen, F. F. Abdi, J. H. van Santen, R. N. Frese, B. Dam, R. van de Krol and J. T. M. Kennis, *J. Phys. Chem. C*, 2014, **118**, 27793–27800.

26 S. Selim, E. Pastor, M. García-Tecedor, M. R. Morris, L. Francàs, M. Sachs, B. Moss, S. Corby, C. A. Mesa, S. Gimenez, A. Kafizas, A. A. Bakulin and J. R. Durrant, *J. Am. Chem. Soc.*, 2019, **141**, 18791–18798.

27 Y. Yang, M. Forster, Y. Ling, G. Wang, T. Zhai, Y. Tong, A. J. Cowan and Y. Li, *Angew. Chemie - Int. Ed.*, 2016, **55**, 3403–3407.

28 L. Jing, J. Zhou, J. R. Durrant, J. Tang, D. Liu and H. Fu, *Energy Environ. Sci.*, 2012, **5**, 6552.

29 M. Barroso, C. A. Mesa, S. R. Pendlebury, A. J. Cowan, T. Hisatomi, K. Sivula, M. Graetzel, D. R. Klug and J. R. Durrant, *Proc. Natl. Acad. Sci. U. S. A.*, 2012, **109**, 15640–15645.

30 I. Grigioni, K. G. Stamplecoskie, E. Selli and P. V Kamat, *J. Phys. Chem. C*, 2015, **119**, 20792–20800.

31 A. Yamakata, C. S. K. Ranasinghe, N. Hayashi, K. Kato and J. J. M. Vequizo, *ACS Appl. Energy Mater.*, 2020, **3**, 1207–1214.

32 T. P. Ruoko, K. Kaunisto, M. Bärtsch, J. Pohjola, A. Hiltunen, M. Niederberger, N. V. Tkachenko and H. Lemmetyinen, *J. Phys. Chem. Lett.*, 2015, **6**, 2859–2864.

33 D. Barreca, G. Carraro, A. Gasparotto, C. Maccato, M. E. A. Warwick, K. Kaunisto, C. Sada, S. Turner, Y. Gönüllü, T.-P. Ruoko, L. Borgese, E. Bontempi, G. Van Tendeloo, H. Lemmetyinen and S. Mathur, *Adv. Mater. Interfaces*, 2015, **2**, 1500313.

34 Y. Ling, G. Wang, J. Reddy, C. Wang, J. Z. Zhang and Y. Li, *Angew. Chem. Int. Ed. Engl.*, 2012, **51**, 4074–4079.

35 B. M. Weckhuysen, *Phys. Chem. Chem. Phys.*, 2003, **5**, 4351.

36 M. A. Bañares, *Catal. Today*, 2005, **100**, 71–77.

37 P. S. Bassi, L. Xianglin, Y. Fang, J. S. C. Loo, J. Barber and L. H. Wong, *Phys. Chem. Chem. Phys.*, 2016, **18**, 30370–30378.

38 A. J. Cowan, W. Leng, P. R. F. Barnes, D. R. Klug and J. R. Durrant, *Phys. Chem. Chem. Phys.*, 2013, **15**, 8772–8.

39 S. R. Pendlebury, A. J. Cowan, M. Barroso, K. Sivula, J. Ye, M. Graetzel, D. R. Klug, J. Tang

and J. R. Durrant, *Energy Environ. Sci.*, 2012, **5**, 6304–6312.

40 H. Dotan, K. Sivula, M. Grätzel, A. Rothschild and S. C. Warren, *Energy Environ. Sci.*, 2011, **4**, 958–964.

41 J. K. Cooper, S. E. Reyes-Lillo, L. H. Hess, C.-M. Jiang, J. B. Neaton and I. D. Sharp, *J. Phys. Chem. C*, 2018, **122**, 20642–20652.

42 S. Y. Smolin, A. K. Choquette, J. Wang, S. J. May and J. B. Baxter, *J. Phys. Chem. C*, 2018, **122**, 115–123.

43 D. Hayes, R. G. Hadt, J. D. Emery, A. A. Cordones, A. B. F. Martinson, M. L. Shelby, K. A. Fransted, P. D. Dahlberg, J. Hong, X. Zhang, Q. Kong, R. W. Schoenlein and L. X. Chen, *Energy Environ. Sci.*, 2016, **9**, 3754–3769.

44 J. Husek, A. Cirri, S. Biswas and L. R. Baker, *Chem. Sci.*, 2017, **8**, 8170–8178.

45 L. M. Carneiro, S. K. Cushing, C. Liu, Y. Su, P. Yang, A. P. Alivisatos and S. R. Leone, *Nat. Mater.*, 2017, **16**, 819–825.

46 E. Pastor, J.-S. Park, L. Steier, S. Kim, M. Grätzel, J. R. Durrant, A. Walsh and A. A. Bakulin, *Nat. Commun.*, 2019, **10**, 3962.

47 J. Schneider and D. Bahnemann, *J. Phys. Chem. C*, 2018, **122**, 13979–13985.

48 N. Serpone, D. Lawless, R. Khairutdinov and E. Pelizzetti, *J. Phys. Chem.*, 1995, **99**, 16655–16661.

49 D. W. Bahnemann, M. Hilgendorff and R. Memming, *J. Phys. Chem. B*, 1997, **101**, 4265–4275.

50 J. Tang, A. J. Cowan, J. R. Durrant and D. R. Klug, *J. Phys. Chem. C*, 2011, **115**, 3143–3150.

51 A. J. Cowan, C. J. Barnett, S. R. Pendlebury, M. Barroso, K. Sivula, M. Graetzel, J. R. Durrant and D. R. Klug, *J. Am. Chem. Soc.*, 2011, **133**, 10134–10140.

52 F. Le Formal, E. Pastor, S. D. Tilley, C. A. Mesa, S. R. Pendlebury, M. Grätzel and J. R. Durrant, *J. Am. Chem. Soc.*, 2015, **137**, 6629–6637.

53 C. A. Mesa, L. Francàs, K. R. Yang, P. Garrido-Barros, E. Pastor, Y. Ma, A. Kafizas, T. E. Rosser, M. T. Mayer, E. Reisner, M. Grätzel, V. S. Batista and J. R. Durrant, *Nat. Chem.*, 2020, **12**, 82–89.

54 Y. Ma, C. A. Mesa, E. Pastor, A. Kafizas, L. Francàs, F. Le Formal, S. R. Pendlebury and J. R. Durrant, *ACS Energy Lett.*, 2016, **1**, 618–623.

55 A. Kafizas, Y. Ma, E. Pastor, S. R. Pendlebury, C. Mesa, L. Francàs, F. Le Formal, N. Noor, M. Ling, C. Sotelo-Vazquez, C. J. Carmalt, I. P. Parkin and J. R. Durrant, *ACS Catal.*, 2017, **7**, 4896–4903.

56 A. Kaouk, T. P. Ruoko, M. Pyeon, Y. Gönüllü, K. Kaunisto, H. Lemmetyinen and S. Mathur, *J. Phys. Chem. C*, 2016, **120**, 28345–28353.

57 J. K. Cooper, Y. Ling, C. Longo, Y. Li and J. Z. Zhang, *J. Phys. Chem. C*, 2012, **116**, 17360–17368.

58 I. H. M. van Stokkum, D. S. Larsen and R. van Grondelle, *Biochim. Biophys. Acta - Bioenerg.*, 2004, **1657**, 82–104.

59 R. E. Rex, Y. Yang, F. J. Knorr, J. Z. Zhang, Y. Li and J. L. McHale, *J. Phys. Chem. C*, 2016, **120**, 3530–3541.

60 I. Grigioni, L. Ganzer, F. V. A. Camargo, B. Bozzini, G. Cerullo and E. Selli, *ACS Energy Lett.*, 2019, **4**, 2213–2219.

61 R. Croce, M. G. Müller, R. Bassi and A. R. Holzwarth, *Biophys. J.*, 2001, **80**, 901–915.

62 C. Slavov, C. Yang, L. Schweighauser, C. Boumrifak, A. Dreuw, H. A. Wegner and J. Wachtveitl, *Phys. Chem. Chem. Phys.*, 2016, **18**, 14795–14804.

63 C. L. Smith, L. L. E. Mears, B. J. Greeves, E. R. Draper, J. Doutch, D. J. Adams and A. J. Cowan, *Phys. Chem. Chem. Phys.*, 2019, **21**, 26466–26476.

64 G. F. Dorlhiac, C. Fare and J. J. van Thor, *PLOS Comput. Biol.*, 2017, **13**, e1005528.

65 V. A. Voelz and V. S. Pande, *Proteins Struct. Funct. Bioinforma.*, 2012, **80**, 342–351.

66 https://optimusfit.org/.